LATTICE MODELING OF CONCRETE FRACTURE INCLUDING MATERIAL SPATIAL RANDOMNESS

Jan Eliáš*, Miroslav Vořechovský*, Jia-Liang Le*

The paper presents stochastic discrete simulations of concrete fracture behavior. The spatial material randomness of local material properties is introduced into a discrete lattice-particle model via an autocorrelated random field generated by the Karhunen-Loève expansion method. The stochastic discrete model is employed to simulate failure of the three-point-bent beams with and without a central notch. The effect of spatial randomness on the peak load and energy dissipation is studied.

Keywords: *lattice model, concrete, fracture, stochastic simulations, material randomness, fracture energy, flexural failure*

1. Introduction

It has been widely recognized that the mechanical properties of materials exhibit spatial variability. Weibull's seminal theory [27] offered a simple and powerful tool to determine the probabilistic distribution of structural strength. However, the applicability of Weibull theory is limited to brittle structures with no redistribution prior to the peak load. Weibull theory lacks any length scale and a rupture of infinitely small volume directly causes the failure of the whole structure. The absence of any characteristic length scale also results in the spurious infinite strength of infinitely small structures [24]. Moreover, Weibull theory assumes that the strength of every material point is independent of its surroundings. However, many structures are made of quasibrittle materials such as concrete, ceramics, rocks or ice. These structures have the ability to partially redistribute released stresses and thus their failure is triggered by the rupture of some representative volume of finite size. Also, the Weibull assumption of independence contradicts the natural expectation that local strengths actually fluctuate continuously inside a structure.

The advantage of Weibull theory comes from the fact that the mechanics of failure do not interact with the stochastic model – only an elastic stress field is needed. The extension of Weibull theory for a finite internal material length scale requires knowledge of changes in the stress field during the redistribution prior to the peak load. This redistribution can be mimicked by the nonlocal Weibull theory formulated in [8] and [5], where the probability of failure of a material point depends not only on its local stress but also on the stress in its surroundings. Therefore, the local stress is replaced by nonlocal stress obtained by averaging of the (local) elastic stress field [3]. The nonlocal Weibull theory agrees with the original local theory for large structural sizes. For intermediate sizes, it predicts higher strengths

* Ing. J. Eliáš, Ph.D., doc. Ing. M. Vořechovský, Ph.D., Institute of Structural Mechanics, Faculty of Civil Engineering, Brno University of Technology, Veveří 331/95; 602 00, Brno; CZ

* Ing. J.-L. Le, Ph.D., Department of Civil Engineering, University of Minnesota, 500 Pilsbury Drive SE, Minneapolis, MN, 55455, USA

than local Weibull theory thanks to the mechanism of stress redistribution. Unfortunately, in the case of very small structures, this theory is not applicable because the approximation or stress redistribution by nonlocal averaging is too simplistic. Even though the nonlocal averaging helps to introduce the material internal length, it is not able to correctly reflect the possible spatial correlations of local material properties.

A laborious method of structural strength estimation is represented by stochastic failure simulations that include a proper treatment of the mechanics of stress redistribution. Such a stochastic analysis can be performed using the finite element method with a sophisticated material constitutive law [22, 26]. The failure of highly heterogeneous materials can also be advantageously modeled via discrete models. These models can be *deterministic* [15, 20, 9] or *stochastic* [14, 1]. In this study, the lattice-particle model developed by G. Cusatis [12] for the modeling of concrete fracture was employed. Spatial material fluctuations are introduced by modeling the material properties as realizations of a random field.

The following Section 2 briefly describes the deterministic mechanical (lattice) model and Section 3 elucidates how spatial randomness is incorporated into the model. The model has been used to obtain numerical results of the failure of notched and unnotched three-point bent beams. The results are presented in Sections 4 (notched beams) and 5 (unnotched beams).

2. The deterministic model

Modeling of the initiation and propagation of cracks in quasibrittle materials exhibiting strain softening has been studied for several decades. Although this is a difficult task complicated by the distributed damage dissipating energy within a fracture process zone (FPZ) of non-negligible size, realistic results have been achieved by several different approaches; see e.g. [7]. The present study is based on the cohesive crack model [2, 17, 7], which is sometimes called the fictitious crack model. It relies on the assumption that the cohesive stress transmitted across a crack is released gradually as a decreasing function of the crack opening, called the cohesive softening curve. Its main characteristic is the total fracture energy, G_{F} – a material constant representing the area under the softening curve.

In heterogeneous materials, the dissipation of energy takes place within numerous meso-level cracks inside the FPZ. Direct modeling of such distributed cracking calls for the representation of the material's meso-level structure. Models capable of efficiently incorporating the concrete meso-structure should be used. For this purpose, the present analysis will be based on the discrete lattice-particle model developed in [12], which is an extension of models presented in [10, 11].

The material is represented by a discrete three-dimensional assembly of rigid cells. The cells are created by tessellation according to pseudo-random locations and the radii of computer generated aggregates/particles. Special kind of tessellation [12] which takes into account diameters of aggregates is used, but inter-particle bonds are determined by standard Delaunay triangulation. Every cell contains one aggregate (Fig. 1a,b). The cells are interconnected by a set of three nonlinear springs (normal – n and two tangential – t_1, t_2) placed at the interfaces between the cells, representing the mineral aggregates in concrete and its surroundings. On the level of rigid cell connection, the cohesive crack model is used to represent cracking in the matrix between the adjacent grains. The inter-particle fracturing is assumed to be of the damage-mechanics type and is modeled using a single damage vari-

able ω applied to all three directions $i = n$, t_1 and t_2. Forces F_i in the springs can thus be evaluated from their extensions Δu_i by

$$F_i = (1 - \omega)\, k_i\, \Delta u_i \tag{1}$$

where k_i is elastic spring stiffness. The damage parameter ω depends on Δu_i and on the previous loading history of each connection. For a detailed description of the connection constitutive law or other model features, see [12]. The confinement effect (present in the full version of the model) is neglected here as it was estimated that confinement does not play any important role in the studied type of experiment.

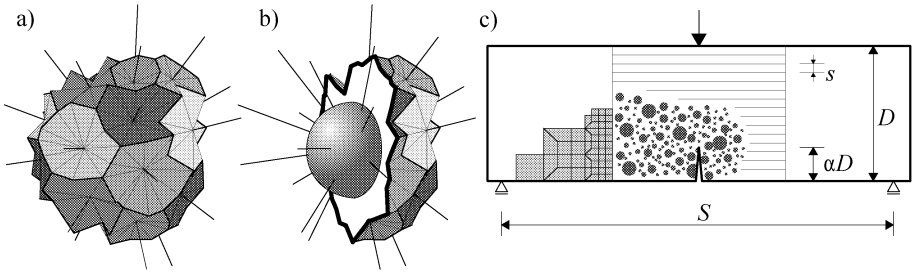

Fig.1: a) One cell of the lattice-particle model and b) its section revealing the aggregate; c) geometry of the beams simulated in three-point-bending

For the purpose of the present numerical study, beams of depths $D = 300\,\mathrm{mm}$, span-depth ratio $S/D = 2.4$ and thickness $t = 40\,\mathrm{mm}$, were modeled. The maximal aggregate diameter was $d_{\max} = 9.5\,\mathrm{mm}$. The minimal grain diameter was selected as 3 mm. Aggregates' diameters within the chosen range were generated using the Fuller curve. The parameters of the connection constitutive law, which were mostly taken to be similar to those in [12], were: matrix elastic modulus $E_\mathrm{c} = 30\,\mathrm{GPa}$; aggregate elastic modulus $E_\mathrm{a} = 90\,\mathrm{GPa}$; meso-level tensile strength $\sigma_\mathrm{t} = 2.7\,\mathrm{MPa}$; meso-level tensile fracture energy $G_\mathrm{t} = 30\,\mathrm{N/m}$; meso-level shear strength $\sigma_\mathrm{s} = 3\,\sigma_\mathrm{t} = 8.1\,\mathrm{MPa}$; meso-level shear fracture energy $G_\mathrm{s} = 480\,\mathrm{N/m}$; meso-level compressive strength $\sigma_\mathrm{c} = 42.3\,\mathrm{MPa}$; $K_\mathrm{c} = 7.8\,\mathrm{GPa}$; $\alpha = 0.25$; $\beta = 1$; $\mu = 0.2$; $n_\mathrm{c} = 2$.

To save computer time, the lattice-particle model covered only the region in which cracking was expected. Surrounding regions of the beams were assumed to remain linear elastic and were therefore modeled by standard 8-node isoparametric finite elements. The elastic constants for these elements were identified by fitting a displacement field with homogeneous strain to displacements of the particle system subjected to low-level uniaxial compression. The macroscopic Young's modulus and Poisson ratio were found to equal $\bar{E} = 34.7\,\mathrm{GPa}$ and $\bar{\nu} = 0.19$. The finite element mesh was connected to the system of particles by introducing interface nodes treated as auxiliary zero-diameter particles [13]. These auxiliary particles have their translational degrees of freedom prescribed by the interpolation of the corresponding translation from the nearest finite element using the shape functions. The rotations of the auxiliary particles were unconstrained.

3. The stochastic model

In the described discrete model, the material properties of each inter-particle connection are assigned according to a stationary autocorrelated random field. The value of the c-th

realization of the discretized field at spatial coordinate $\boldsymbol{x}$ is denoted $\boldsymbol{H}^c(\boldsymbol{x})$. For a given coordinate $\boldsymbol{x}_0$, $\boldsymbol{H}(\boldsymbol{x}_0)$ is a random variable H of the cumulative distribution function (cdf) $F_{\mathrm{H}}(h)$. Since the random field considered here is stationary, the cdf $F_{\mathrm{H}}(h)$ is identical for any position $\boldsymbol{x}_0$. Recent studies by Bažant and co-workers [6, 4] have shown that when H represents the strength of a quasibrittle material, $F_{\mathrm{H}}(h)$ can be approximated by a Gaussian distribution onto which a power-law tail is grafted from the left at a probability of about $10^{-4} \div 10^{-3}$

$$F_{\mathrm{H}}(r) = \begin{cases} r_{\mathrm{f}} \left(1 - \mathrm{e}^{-\langle h/s_1 \rangle^m}\right) & 0 \le h \le h_{\mathrm{gr}} \ , \qquad (2a) \\ F_{\mathrm{H}}(h_{\mathrm{gr}}) + \dfrac{r_{\mathrm{f}}}{\delta_{\mathrm{G}}\sqrt{2\pi}} \displaystyle\int_{h_{\mathrm{gr}}}^{h} \mathrm{e}^{-(h-\mu_{\mathrm{G}})^2/(2\,\delta_{\mathrm{G}}^2)}\,\mathrm{d}h & h > h_{\mathrm{gr}} \qquad (2b) \end{cases}$$

where $\langle x \rangle = \max(x, 0)$, $s_1 = s_0\, r_{\mathrm{f}}^{1/m}$, m is the Weibull modulus (shape parameter) and s_0 is the scale parameter of the Weibull tail, μ_{G} and δ_{G} are the mean value and the standard deviation of the Gaussian distribution that provides the Gaussian core. The Weibull-Gauss juncture at the point at h_{gr} requires that $(\mathrm{d}F_{\mathrm{H}}/\mathrm{d}h)|_{h_{\mathrm{gr}}^+} = (\mathrm{d}F_{\mathrm{H}}/\mathrm{d}h)|_{h_{\mathrm{gr}}^-}$. r_{f} is a scaling parameter normalizing the distribution to satisfy $F_{\mathrm{H}}(\infty) = 1$. The distribution has 4 independent parameters in total.

The spatial fluctuation of the field is characterized through an autocorrelation function. It determines the spatial dependence pattern between the random variables at any pair of nodes. The correlation coefficient ρ_{ij} between two field variables at coordinates $\boldsymbol{x}_i$ and $\boldsymbol{x}_j$ can be assumed to obey the squared exponential function

$$\rho_{ij} = \exp\left[-\left(\frac{\|\boldsymbol{x}_i - \boldsymbol{x}_j\|}{d}\right)^2\right] \qquad (3)$$

It introduces a new parameter d called the autocorrelation length.

To digitally simulate the stationary random field described by the random variable cdf F_{H} and correlation length d in the discrete model, N realizations of the discretized random field $\boldsymbol{H}^0(\boldsymbol{x}), \boldsymbol{H}^1(\boldsymbol{x}), \ldots, \boldsymbol{H}^{N-1}(\boldsymbol{x})$ must be generated at the facet centers of the model. This is achieved using the Karhunen-Loève expansion based on the spectral decomposition of covariance matrix $\boldsymbol{C}$, where $C_{ij} = \rho_{ij}$. This procedure decomposes the correlated Gaussian variables $\widehat{\boldsymbol{H}}(\boldsymbol{x}_i)$ into independent standard Gaussian variables ξ_k that are easy to generate. The c-th realization of the Gaussian random field $\widehat{\boldsymbol{H}}^c(\boldsymbol{x})$ is then obtained using K standard Gaussian random variables by the following expression

$$\widehat{\boldsymbol{H}}^c(\boldsymbol{x}) = \sum_{k=1}^{K} \sqrt{\lambda_k}\, \xi_k^c\, \boldsymbol{\psi}_k(\boldsymbol{x})$$

where λ and $\boldsymbol{\psi}$ are the eigenvalues and eigenvectors of the covariance matrix $\boldsymbol{C}$. Value K is the number of eigenmodes/variables considered. In practice, it suffices to employ only a reduced number of eigenmodes $K \ll$ order of $\boldsymbol{C}$. In particular, K can be selected so that $\sum_{k=1}^{K} \lambda_k$ corresponds to about 99 % of the trace of the covariance matrix $\boldsymbol{C}$ [23]. The vectors of independent standard Gaussian variables $\boldsymbol{\xi}$ are generated by Latin Hypercube Sampling using the mean value of each subinterval. The spurious correlation of the variables is then minimized by reordering their K realizations [25].

A non-Gaussian random field can be generated by isoprobabilistic transformation of the underlying Gaussian field as

$$\boldsymbol{H}^c(\boldsymbol{x}) = F_{\mathrm{H}}^{-1}(\Phi(\widehat{\boldsymbol{H}}^c(\boldsymbol{x}))) \tag{5}$$

where Φ is standard Gaussian cdf. Such a transformation, however, distorts the correlation structure of the field. Thus, when generating Gaussian field $\widehat{\boldsymbol{H}}$, the correlation coefficients must be modified [23]. This is performed here using the approximate method [18].

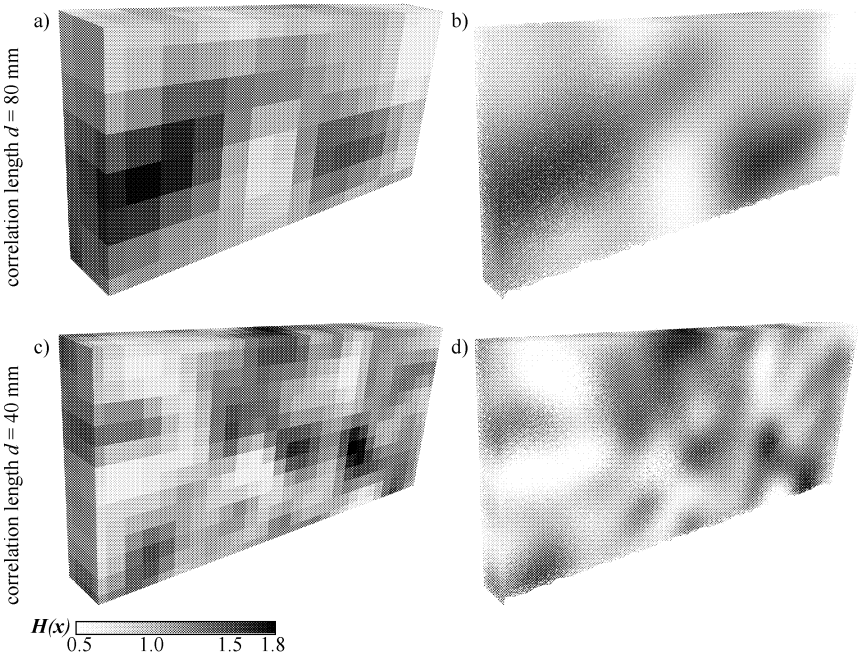

Fig.2: Left : one realization of the autocorrelated random field $\boldsymbol{H}$ *on a grid of spacing* $d/3$ *for* $d = 80\,mm$ *(top) and* $d = 40\,mm$ *(bottom); right : realization of field* $\boldsymbol{H}$ *at the element centers of the lattice-particle model*

The realizations of the random field need to be evaluated for every shared facet (interparticle bond) of the discrete mechanical model (at its center). This can be computationally extremely demanding for a large number of facets (large covariance matrix) and a short correlation length d (many eigenvalues needed, large K). Therefore,the expansion optimal linear estimation method – EOLE [19] was adopted, as it can significantly reduce the duration of random field generation. Instead of using the facet centers, the random field is initially generated on a regular grid of nodes with spacing $d/3$ (see Fig. 2). The values of the random field at the facets are then obtained from the expression

$$\widehat{\boldsymbol{H}}^c(\boldsymbol{x}) = \sum_{k=1}^{K} \frac{\xi_k^c}{\sqrt{\lambda_k}}\, \boldsymbol{\psi}_k^{\mathrm{T}}\, \boldsymbol{C}_{\mathrm{xg}} \tag{6}$$

where λ and $\boldsymbol{\psi}$ are now eigenvalues and eigenvectors of the covariance matrix of the grid nodes, and $\boldsymbol{C}_{\mathrm{xg}}$ is a covariance matrix between the facet center at coordinates $\boldsymbol{x}$ and the grid nodes. After the Gaussian random field values at the facet centers are obtained by EOLE (Eq. 6), they need to be transformed to the non-Gaussian space by Eq. 5.

Besides the significant time savings, another advantage of using EOLE is that one can simply use the same field realization for several different granular positions. By keeping the c-th realization of decomposed variables $\boldsymbol{\xi}^c$ unchanged, the field realization can be adapted for any configuration of the facets in the discrete model.

Structural strength of a quasibrittle material is typically governed by two important material properties, namely the material strength and fracture energy. Realistic fracture models should therefore incorporate the random spatial variability of at least these two variables. It is reasonable to consider the material strength as being fully correlated with the fracture energy [14]. Furthermore, the proposed lattice model also includes the shear strength f_s and mode-II fracture energy G_s, which are again assumed to be fully correlated with the tensile strength f_t and mode-I fracture energy G_t, respectively. Assuming identical coefficients of variation (cov), the same realizations of the random field can be used to generate the values of material strengths and fracture energies. For X substituted by any of the four mentioned mechanical properties, the following can be written

$$X(\boldsymbol{x}) = \bar{X}\,\boldsymbol{H}(\boldsymbol{x}) \tag{7}$$

where $\bar{X}$ stands for the mean value of the particular property. The mean value of the (field) random variable H has to equal 1.

In this study, the following parameters of the Weibull-Gauss grafted distribution (Eq. 2a) were used: $m = 24$; $s_1 = 0.486\,\mathrm{MPa}$; $h_\mathrm{gr} = 0.364\,\mathrm{MPa}$; $\delta_\mathrm{G} = 0.25$. These values provided the overall mean value μ_H=1; standard deviation δ_H ≈0.25 and the grafting probability $F_\mathrm{H}(h_\mathrm{gr}) \approx 10^{-3}$. Two correlation lengths d were considered: a shorter length $d_4 = 40\,\mathrm{mm}$ (according to [14]) and a longer length $d_8 = 80\,\mathrm{mm}$ (according to [22]). The computation was performed with $N = 24$ realizations of the random field for each correlation length.

4. Simulations of the bending of notched beams

The first set of beams (depth $D = 300\,\mathrm{mm}$, span $S = 2.4\,D$, thickness $t = 40\,\mathrm{mm}$) loaded in three-point-bending were modeled with a central notch up to 1/6 of its depth. Ten deterministic simulations were computed. These simulations exhibited a certain scat-

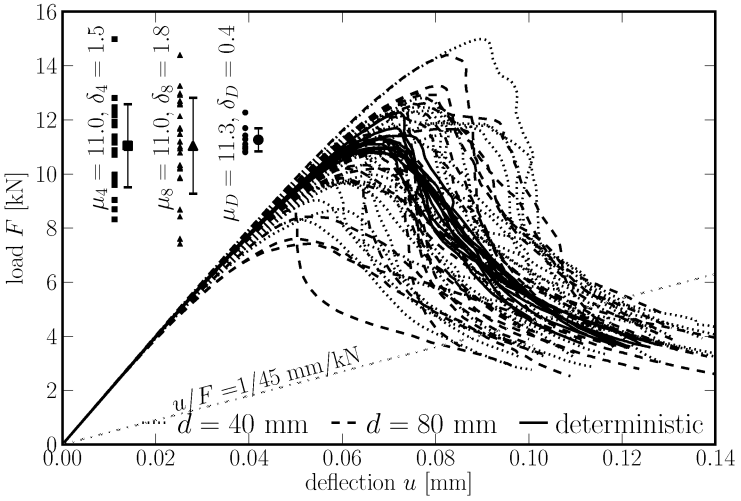

Fig.3: Load-deflection curves for simulations of notched TPB beams

ter because the pseudo-random granular positions differed for each realization. For both correlation lengths, 40 and 80 mm, 24 simulations with spatial material randomness were performed. Besides the scatter due to the applied randomness, additional scatter comes again from random granular positions that differed for every realization and every model type, i.e. i-th realizations of deterministic and both stochastic models had different granular positions. All the simulations were terminated when the magnitude of the loading force dropped to 1/3 of the maximal reached load $F_{\max}$. To ensure numerical stability in the presence of softening, the simulations were controlled by prescribing an increase in the crack mouth opening displacement (CMOD) in every step.

The notch present in the model induces a stress concentration at its tip. As a result, high stresses only occur in a small area above the notch tip and thus cracks always initiate and propagate from that location. In stochastic calculations with rather a large correlation length, local strength fluctuations within the region of high stresses diminish because of the imposed spatial correlation. The peak load $F_{\max}$ thus depends mostly on a single value of the random field realization at the notch tip location. In other words, a random field with a correlation length greater than the length/width of the FPZ can be, in the vicinity of the crack tip, viewed as a random constant – the random field becomes a random variable in that region.

The obtained load-deflection curves are shown in Fig. 3. The figure also shows the maximal loads $F_{\max}$ in its upper left corner. The effect of the spatial strength fluctuations on the mean value of maximum load is negligible. The mean value of $F_{\max}$ is $\mu_{\mathrm{D}} = 11.3\,\mathrm{kN}$ for the deterministic calculation and $\mu_4 = \mu_8 = 11.0\,\mathrm{kN}$ for stochastic simulations with $d = 40$ and 80 mm. However, the standard deviations of the peak load are significantly influenced by the material randomness. The standard deviation of deterministic calculations (given solely by random aggregate position) is $\delta_D = 0.4\,\mathrm{kN}$. A significant increase in the standard deviation is observed for both correlation lengths: $\delta_4 = 1.5\,\mathrm{kN}$ ($d = 40\,\mathrm{mm}$) and $\delta_8 = 1.8\,\mathrm{kN}$ ($d = 80\,\mathrm{mm}$). Since the maximal load of the beam is given by the local meso-level strength of a small area above the notch tip, the authors believe that the correlation length does not influence the standard deviation (unless it is so small that material parameters vary significantly inside the FPZ).

For several selected realizations, the computed damage patterns (damage parameter ω from Eq. 1) at the peak load and at the termination of the simulations are shown in Fig. 4 together with the corresponding random field realization. Even though one can notice that the crack is slightly attracted (repelled) by areas of low (high) strength, the macrocrack trajectory is similar to that present in the deterministic case (dictated by the singular stress field).

In order to compare energy dissipation in the beams, it is necessary to determine simulation stages where the same portion of the ligament has already been damaged. Therefore, a stage was selected when equivalent crack lengths (according to LEFM) are equal. Thus, at that (reference) stage all the models should have the same (reference) compliance, chosen as 1/45 mm/kN (Fig. 3). The depth of each specimen was divided into horizontal stripes of depth s (Fig. 1c). All the energy dissipated during inter-particle contact within a specific stripe was summed into the variable G_{d}. One can normalize that energy by ligament area as $g_{\mathrm{d}} = G_{\mathrm{d}}/(s\,t)$. The mean values and standard deviations of g_{d} are plotted in Fig. 5 for every stripe at the peak load and at the reference compliance stages. The figure confirms

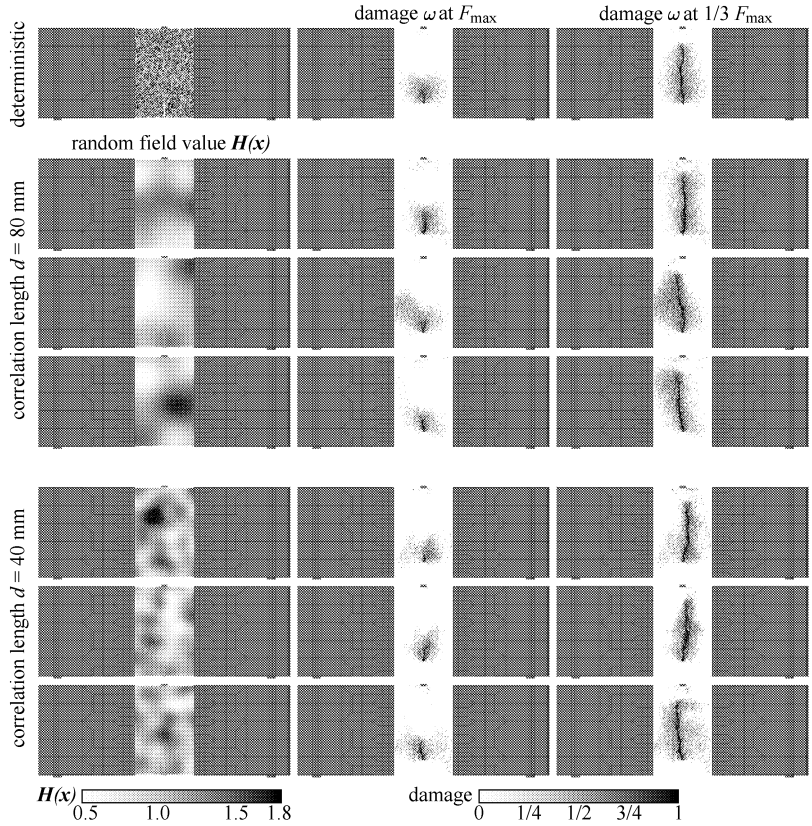

Fig.4: Realizations of random field $\boldsymbol{H}$ *(left) and corresponding damage patterns developed in bent notched beams at the peak force (middle) and after the load dropped to* 1/3 *of its maximum (right)*

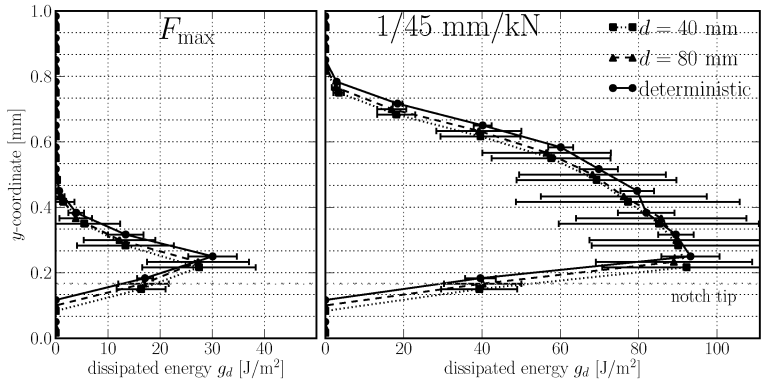

Fig.5: Energy g_{d} *per unit of ligament area dissipated in notched beams up to a) maximal load and b) the reference beam compliance* 1/45 *mm/kN as a function of the vertical position in the beam*

that the mean energy dissipation in notched tests does not change when spatial material randomness is applied. As with the peak force behavior, standard deviations of dissipated energy increase when randomness is present.

5. Simulations of the bending of unnotched beams

The second simulation set focused on the bending of unnotched beams where cracks initiate from a smooth bottom surface. Ten deterministic simulations and $N = 24$ simulations with a random field for each correlation length were performed. To control the simulation, one needs to find a monotonically increasing variable; here again the CMOD was used. For unnotched beams with spatially fluctuating meso-level strength, the location of the macrocrack and thus the position of the crack mouth is not known in advance. Therefore, several short overlapping intervals were monitored simultaneously and the controlling CMOD was chosen to be the maximum one among all of them. Note that another possible option for a controlling variable might be the total energy dissipation in the specimen [16].

The variations in the position of the crack mouth of the macrocrack are documented in Fig. 6. The figure demonstrates the fundamental difference between notched and unnotched simulations. When no notch is present, the high-level stress region is much larger, located along the bottom central part of the specimen. Material strength and fracture energy fluctuate within the region and allow the macrocrack to 'choose a weak spot' to initiate from. The higher the distance from the midspan, the lower the tensile stress that appears. During the process of crack(s) formation, the stress field with a certain ability of redistribution increases towards the barrier (with randomly varying strength and energy). The crack would start far from the midspan only if the material strength (and energy) of all points closer to the midspan were higher than in the surrounding region. It is thus to be expected (and this is confirmed by Fig. 6) that short correlation length, resulting in fluctuations that generate the weak spots more frequently, shrinks the zone where the macrocrack initiates. Indeed, the initiation zone for correlation length $d = 80\,\text{mm}$ is wider than for $d = 40\,\text{mm}$.

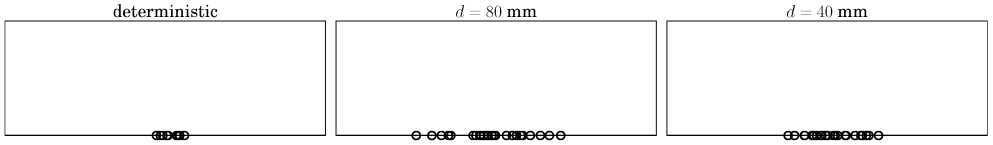

Fig.6: Points of crack initiation in unnotched beams for various degrees of randomness

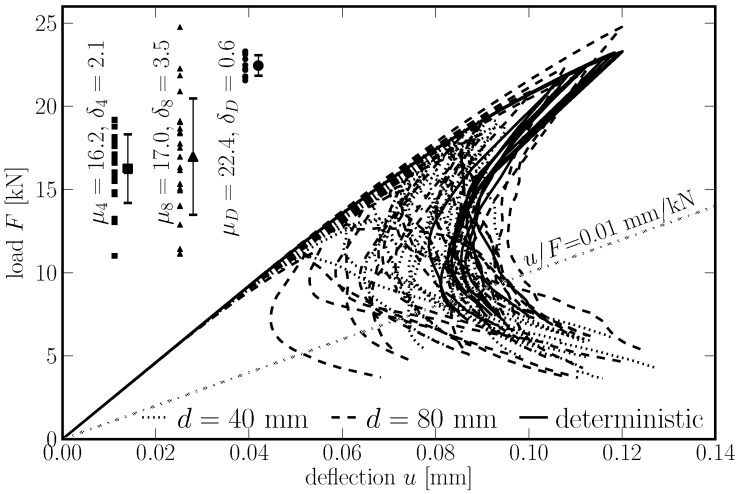

Fig.7: Load-deflection curves for simulations of unnotched TPB beams

The load-deflection curves obtained from all the performed simulations are plotted in Fig. 7. The upper left corner shows the mean values and standard deviations of the peak load $F_{\max}$. The more the local strength fluctuates, the weaker the spot that is statistically present and thus the lower the mean value: $\mu_{\mathrm{D}} = 22.4\,\mathrm{kN}$ (deterministic), $\mu_8 = 17.0\,\mathrm{kN}$ ($d = 80\,\mathrm{mm}$), $\mu_4 = 16.2\,\mathrm{kN}$ ($d = 40\,\mathrm{mm}$). The standard deviation of the maximal force is low for the deterministic set, where $\delta_{\mathrm{D}} = 0.6\,\mathrm{kN}$ ($\mathrm{cov}_{\mathrm{D}} = 2.7\,\%$). It increases rapidly for the correlation length 80 mm, to $\delta_8 = 3.5\,\mathrm{kN}$ ($\mathrm{cov}_8 = 21\,\%$). When the fluctuation rate increases further ($d = 40\,\mathrm{mm}$), the standard deviation of $F_{\max}$ decreases back to $\delta_4 = 2.1\,\mathrm{kN}$ ($\mathrm{cov}_4 = 13\,\%$). This trend simply arises because the standard deviation of the local strength in the weakest spot inside a given fixed region decreases with decreasing correlation length. Theoretically, the maximal standard deviation of $F_{\max}$ should be obtained for $d \approx \infty$ (a situation when the random field can be represented by a random variable – a random constant over the specimen volume).

Fig. 8 presents several selected realizations of the random field $\boldsymbol{H}$ and the computed damage patterns. One can see that the damage patterns differ for different levels of randomness. In the deterministic case, the damaged region at the peak load stage continuously spans the whole bottom area and the damage intensity directly depends on the distance from the midspan. For a random local strength and local fracture energy, the damage regions

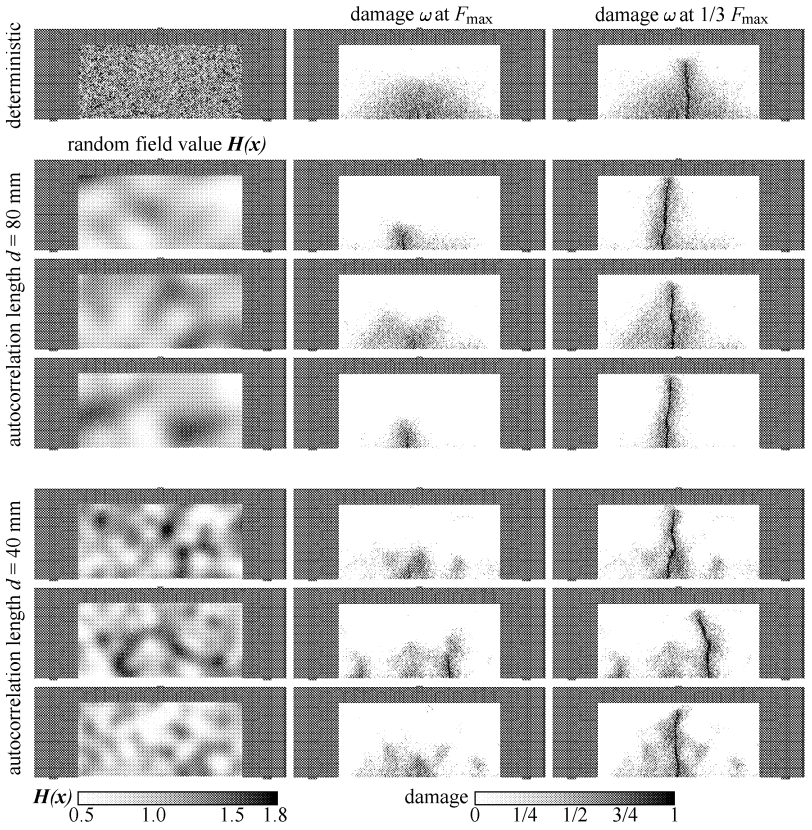

Fig.8: Realizations of random field $\boldsymbol{H}$ (left) and corresponding damage patterns developed in bent unnotched beams at peak force (middle) and after the load dropped to 1/3 of its maximum (right)

are more localized around low random field values. There is usually one such region for correlation length $d = 40\,\text{mm}$ and several low strength regions for $d = 80\,\text{mm}$.

To compare the energy dissipations, a reference compliance was again chosen to mark stages with the same LEFM crack length. The reference compliance now equals 1/100 mm/kN (Fig. 7). Contrary to the results from notched simulations, the summation of total energy dissipated in stripes (per unit ligament area) is dependent on material randomness. In Fig. 9, deterministic calculations show higher values of dissipated energy g_d both for the peak force stage and for the stage at the reference compliance. This is caused by two factors: i) the localized macrocrack propagates in stochastic simulations through areas of lower meso-level strength and meso-level fracture energy, thus less energy is dissipated in total; ii) distributed pre-peak cracking outside the macrocrack occurs mostly in deterministic simulations and thus it increases its total energy dissipation. Note that from about the middle of the specimens depth upwards, the energy dissipations of deterministic and stochastic simulations match each other. This is because the crack at that depth cannot choose the weak region as it has already localized, and the stress field forces the crack to grow from the current crack tip; thus, no pre-peak distributed cracking takes place there.

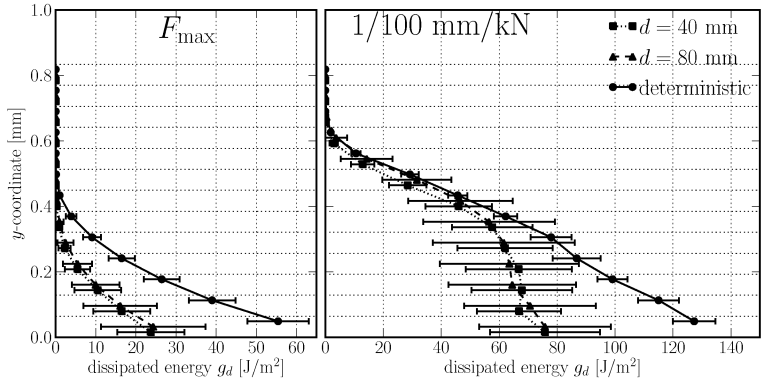

Fig.9: Energy per unit ligament area dissipated in unnotched beams up to a) maximal load and b) reference beam compliance 1/100 mm/kN as a function of the vertical position in the beam

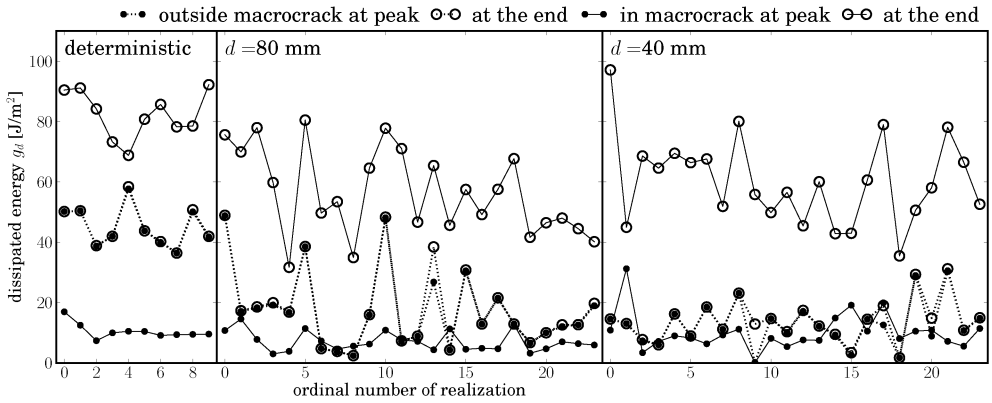

Fig.10: Energy dissipation inside and outside the macrocrack at the peak load and at the reference compliance stages for every simulation

Finally, let us focus on a deeper analysis of the energy dissipation along the bottom surface. In the bottom boundary stripe of width $2\,d_{\max} = 19\,\text{mm}$, the dissipated energies (per unit ligament area) inside and outside the macrocrack were evaluated for stages at the peak load and at the reference compliance. These values are plotted separately in Fig. 10 for each simulation. Curves for energy dissipation *outside* the macrocrack at the peak load and at the end almost coincide. This documents that distributed cracking outside the macrocrack in the bottommost layer after the peak is reached is close to zero, crack is localized. The amount of energy dissipated *outside* a macrocrack is much higher for the deterministic simulations than for those with random fields. Some of the simulations for $d = 80\,\text{mm}$ reached the value of the deterministic model, which can be explained by the absence of a local weak spot and subsequent extensive pre-peak distributed cracking (see Fig. 8, third row). The energy dissipated *inside* the macrocrack at the reference compliance is clearly higher in the deterministic case than in the stochastic one. This is due to the positive correlation between local meso-level energy and meso-level strength at the inter-particle bonds. Since the macrocrack propagates through locally weaker areas, it also dissipates less energy there. Aspects related to correlation between local tensile strength and fracture energy have been discussed in [21].

6. Conclusions

The influence of material spatial randomness on peak load and energy dissipation was analyzed using a discrete lattice-particle model that reflects the meso-scopic structure of concrete, i.e. its aggregate composition. Spatial material randomness was introduced by the simultaneous scaling of the local meso-level strength and fracture energy of inter-particle bonds by realizations of an autocorrelated random field. Two basic cases of three-point-bent beams were investigated: i) beams with a notch and ii) beams without a notch (the modulus of rupture test). The numerical results generally confirm theoretical expectations.

It has been found that:

- for simulations with a sufficiently deep notch, the crack is forced to start at the notch tip. Therefore, the mean value of the maximal load for notched beam simulations does not change when material spatial randomness applies. However, the standard deviation of the maximal load increases when strength randomness is introduced. Also, the energy dissipations in deterministic and random media exhibit the same mean but an increasing standard deviation for the random cases.
- In the case of unnotched beams, the macrocrack initiates in a locally weaker spot. The shorter the correlation length of material properties, the weaker is the statistically weakest initiation spot and thus the lower is the mean maximum load. Standard deviations of the maximal load increase when randomness is applied; however, shorter correlation lengths lead to a decrease in the standard deviation.
- Energy dissipated in unnotched beams is dependent on the randomness of the material. Two effects responsible for the dependency were identified. i) A change in the dissipated energy due to the correlation of the local meso-level fracture energy and the low meso-level strength of the inter-particle bonds through which the macrocrack propagates. Depending on the sign of the energy-strength cross-correlation, this effect may increase or decrease the dissipated energy. For the current settings of the model, the lower is the local meso-level strength, the lower is also the local fracture energy and the lower is

the energy dissipated inside the macrocrack. ii) The pre-peak distributed cracking has a tendency to localize only in weaker areas and thus the material dissipates less energy outside the macrocrack when the random field is applied.

Acknowledgments

The financial support received from the Ministry of Education, Youth and Sports of the Czech Republic under Project No. LH12062 is gratefully acknowledged.

References

[1] Alava M.J., Nukala P.K.V.V., Zapperi S.: Statistical models of fracture, Advances in Physics, Vol. 55 (2006), No. 3–4, pp. 349–476

[2] Barenblatt G.I.: Mathematical theory of equilibrium cracks in brittle fracture. Advances in Applied Mechanics, Vol. 7 (1962), pp. 55–129

[3] Bažant Z.P., Jirásek M.: Nonlocal integral formulations of plasticity and damage: Survey of progress, ASCE's Journal of Engineering Mechanics, Vol. 128 (2002), No. 11, pp. 1119–1149

[4] Bažant Z.P., Le J.-L., Bazant M.Z.: Scaling of strength and lifetime distributions of quasibrittle structures based on atomistic fracture mechanics, Proceeding of the National Academy of Sciences, USA, Vol. 106 (2009), No. 28, pp. 11484–11489

[5] Bažant Z.P., Novák D.: Probabilistic nonlocal theory for quasibrittle fracture initiation and size effect. I. Theory, ASCE's Journal of Engineering Mechanics, Vol. 126 (2000), No. 2, pp. 166–174

[6] Bažant Z.P., Pang S.-D.: Activation energy based extreme value statistics and size effect in brittle and quasibrittle fracture, Journal of the Mechanics and Physics of Solids, Vol. 55 (2007), pp. 91–131

[7] Bažant Z.P., Planas J.: Fracture and size effect in concrete and other quasibrittle materials, CRC Press, 1998

[8] Bažant Z.P., Xi Y.: Statistical size effect in quasi-brittle structures: II. Nonlocal theory, ASCE's Journal of Engineering Mechanics, Vol. 117 (1991), No. 7, pp. 2623–2640

[9] Bolander J.E., Saito S.: Fracture analyses using spring networks with random geometry, Engineering Fracture Mechanics, Vol. 61 (1998), pp. 569–591

[10] Cusatis G., Bažant Z., Cedolin L.: Confinement-shear lattice model for concrete damage in tension and compression: I. theory, ASCE's Journal of Engineering Mechanics, Vol. 129 (2003), pp. 1439–1448

[11] Cusatis G., Bažant Z., Cedolin L.: Confinement-shear lattice csl model for fracture propagation in concrete, Computer Methods in Applied Mechanics and Engineering, Vol. 195 (2006), pp. 7154–7171

[12] Cusatis G., Cedolin L.: Two-scale study of concrete fracturing behaviour, Engineering Fracture Mechanics, Vol. 6 (2007), pp. 3–17

[13] Eliáš J., Bažant Z.: Fracturing in concrete via lattice-particle model, In Onate, E., and Owen, D., editors, 2nd international conference on particle-based methods – fundamentals and applications, p. 12, Barcelona, Spain, 2011, CD ROM

[14] Grassl P., Bažant Z.P.: Random lattice-particle simulation of statistical size effect in quasi-brittle structures failing at crack initiation, ASCE's Journal of Engineering Mechanics, Vol. 135 (2009), pp. 85–92

[15] Grassl P., Rempling R.: A damage-plasticity interface approach to the meso-scale modelling of concrete subjected to cyclic compressive loading, Engineering Fracture Mechanics, Vol. 75 (2008), pp. 4804–4818

[16] Gutiérrez M.A.: Energy release control for numerical simulations of failure in quasi-brittle solids, Communications in Numerical Methods in Engineering, Vol. 20 (2004), No. 1, pp. 19–29

[17] Hillerborg A., Modéer M., Petersson P.-E.: Analysis of crack formation and crack growth in concrete by means of fracture mechanics and finite elements, Cement and Concrete Research, Vol. 6 (1976), pp. 773–782

[18] HongShuang L., ZhenZhou L., XiuKai Y.: Nataf transformation based point estimate method, Chinese Science Bulletin, Vol. 53 (2008), No. 17, pp. 2586–2592
[19] Li C.-C., Kiureghian A.D.: Optimal discretization of random fields, ASCE's Journal of Engineering Mechanics, Vol. 119 (1993), No. 6, pp. 1136–1154
[20] Van Mier J.G.M., Van Vliet M.R.A.: Influence of microstructure of concrete on size/scale effects in tensile fracture, Engineering Fracture Mechanics, Vol. 70 (2003), pp. 2281–2306
[21] Vořechovský M., Novák D.: Modeling statistical size effect in concrete by the extreme value theory, In Walraven J., Blaauwendaad J., Scarpas T., and Snijder B., editors, 5$^{\text{th}}$ International Ph.D. Symposium in Civil Engineering, held in Delft, The Netherlands, Vol. 2, pp. 867–875, London, UK, 2004, A.A. Balkema Publishers, ISBN 90 5809 676 9
[22] Vořechovský M.: Interplay of size effects in concrete specimens under tension studied via computational stochastic fracture mechanics, International Journal of Solids and Structures, Vol. 44 (2007), pp. 2715–2731
[23] Vořechovský M.: Simulation of simply cross correlated random fields by series expansion methods, Structural Safety, Vol. 30 (2008), pp. 337–363
[24] Vořechovský M.: Incorporation of statistical length scale into Weibull strength theory for composites, Composite Structures, Vol. 92 (2010), No. 9, pp. 2027–2034
[25] Vořechovský M., Novák D.: Correlation control in small-sample Monte Carlo type simulations I: A simulated annealing approach, Probabilistic Engineering Mechanics, Vol. 24 (2009), pp. 452–462
[26] Vořechovský M., Sadílek V.: Computational modeling of size effects in concrete specimens under uniaxial tension, International Journal of Fracture, Vol. 154 (2008), pp. 27–49
[27] Weibull W.: The phenomenon of rupture in solids, In Royal Swedish Institute of Engineering Research, Vol. 153 (1939), pp. 1–55, Stockholm

Received in editor's office: September 18, 2012
Approved for publishing: September 25, 2013